High Fermi-level spin polarization in the (Bi_{1−x}Sb_{x})_{2}Te_{3} family of topological insulators: A point contact Andreev reflection study

K. Borisov, C.-Z. Chang, J. S. Moodera, and P. Stamenov

Phys. Rev. B **94**, 094415 — Published 13 September 2016

DOI: 10.1103/PhysRevB.94.094415

High Fermi level spin polarisation in the $(Bi_{1-x}Sb_x)_2Te_3$ family of topological insulators - A Point Contact Andreev Reflection study

K. Borisov* and P. Stamenov
School of Physics and CRANN, Trinity College, Dublin 2, Ireland

C.-Z. Chang and J. S. Moodera
Franics Bitter Magnet Laboratory, Massachusetts Institute of Technology, Cambridge, MA, United States
(Dated: August 2, 2016)

Point Contact Andreev Reflection spectroscopy is employed to extract the effective Fermi level spin polarisation of three distinct compositions from the $(Bi_{1-x}Sb_x)_2Te_3$ topological insulator family. The end members, Bi_2Te_3 and Sb_2Te_3, exhibit high polarisation of 70(4) % and 57(3) %, respectively. High-field ($\mu_0 H = 14\,\mathrm{T}$) point-contact spectroscopy shows the carrier depletion close to the Fermi level for these two compositions with small bandgaps of 0.40(4) meVand 0.28(2) meV, respectively. The almost fully suppressed bulk conductivity in the $(Bi_{0.18}Sb_{0.82})_2Te_3$ results in even higher spin polarisation of 83(9) %. Further, it is demonstrated that magnetic doping with Cr and V tends to reduce the spin polarisation values with respect to the ones of the pure compositions. $Bi_{1.97}Cr_{0.03}Te_3$, $Sb_{1.975}Cr_{0.025}Te_3$, $Bi_{1.975}V_{0.025}Te_3$, and $Sb_{1.97}V_{0.03}Te_3$ exhibit spin polarisation of 52 %, 52 %, 58 %, and 50 %, respectively. In view of the rather high effective polarisation, non-magnetic topological insulators close to $(Bi_{0.18}Sb_{0.82})_2Te_3$ may provide a path towards the characterization of pair-breaking mechanisms in spin triplet superconductors.

Keywords: Topological Insulators, Andreev Reflection, Point Contact Spectroscopy

I. INTRODUCTION

The generation and detection of highly spin-polarised currents is of crucial importance to the field of spin electronics. Spin generators with high spin polarisation and low magnetisation are highly sought after. High spin polarisation improves the tunnelling magnetoresistance (TMR) effect in magnetic tunnel junctions (MTJs), whereas decreased magnetisation generally lowers the switching or precession currents in spin-transfer torque based devices. Topological insulators[1], spin-polarised antiferromagnets[2] and compensated ferrimagnets[3] are some classes of materials that can satisfy these seemingly contradicting requirements. Indeed, magnetization switching through giant spin-orbit torque has been demonstrated in topological insulators (TIs) bilayer structure[4], and voltage control of the spin-orbit torque of magnetic topological insulators was recently achieved[5]. TIs possess helically spin-polarized Dirac cone for their surface states. The spin momentum locking is extremely beneficial as a mere switching of a ballistic current direction provides the opposite spin polarization of the current. Although the spin polarized Dirac cone have been studied in various TIs by angle-resolved and spin-resolved photoemission spectroscopy (ARPES and SRPES)[6], the evidence for direct electrical detection is scarce. Direct electric current detection of the TI spin polarized surface states have recently been reported by magnetoresistance measurements[7] and non-local spin injection[8–10]. Here we report on the direct spin polarized current detection by Point Contact Andreev Reflection (PCAR) spectroscopy. Among the three well-established direct spin polarisation measurement techniques (SRPES, spin-polarized tunnelling[11] and Andreev reflection[12]), PCAR has the distinct advantage that it can be used to evaluate the ballistic spin polarisation in a very narrow energy window centered at the Fermi level[13], P. While the primary focus of this work is PCAR spin polarization measurements on high-quality thin films of the compositions Bi_2Te_3, Sb_2Te_3, and $(Bi_{0.18}Sb_{0.82})_2Te_3$, high-field point contact spectroscopy is also studied, in order to demonstrate the low-temperature semiconducting behavior of the two end compositions and allows for the extraction of their gap values. Finally, the spin polarization in four magnetically-doped TIs ($Bi_{1.97}Cr_{0.03}Te_3$, $Sb_{1.975}Cr_{0.025}Te_3$, and $Bi_{1.975}V_{0.025}Te_3$, and $Sb_{1.97}V_{0.03}Te_3$) is probed to find substantially reduced values when compared to the same in the original compositions.

II. EXPERIMENTAL DETAILS

PCAR[12], spin-polarised tunnelling, spin-resolved photoemission spectroscopy and spin-resolved field emission spectroscopy are just some of the techniques applicable towards the measurement of spin polarisation. PCAR is one of the most versatile ones, among these, for it has the ability to probe not only the diffusive, but also the ballistic definition of the spin polarisation in the meV vicinity of the Fermi level[13]. The experimental configuration utilized here is known as the needle-anvil approach, where a shear-cut superconducting niobium tip (Nb) lands on the sample. The "landing" procedure in our experimental setup is fully automatic and performed using a vertical atto**cube**$^{\mathrm{TM}}$ piezo stepper. Negative feedback based on zero-bias differential conductance is used to control the effective size of the contact. Whenever needed, horizontal stepping is performed as well in order to ensure that a pristine (unscratched) area of the sample is always probed. Direct bias-dependent differential conductance measurements are taken instead of sampling the DC current-voltage characteristics and computing their numerical derivatives. This preferred approach has the advantage of better signal-to-noise ratio, due primarily to the use of lock-in amplifiers (LIA) and the corresponding narrowbanding and optimal pre-amplifier use. Furthermore, the differential spectra are observed and recorded in real time, at a rate of 1 Hz. This permits more sophisticated post-processing, where the contact drifts can be essentially eliminated and their influence on the further data analysis minimized. Low-frequency (0.5 Hz) analog triangular waveform is modulated by the internal synchronous oscillator of a LIA (1.23 kHz). The modulation frequency is chosen high-enough to minimize the $1/f$-noise contributions of the JFET pre-amplifiers, but at the same time low-enough, in order to keep to a minimum the signal dephasing due to the spurious cable inductance and capacitance. The modulated voltage waveform is fed in the contact and the current is pre-amplified at variable gain and band filtered, at 6 dB/octave, before being recorded by the LIAs. Two synchronized LIAs measure and transfer data concurrently on the upward and downward trend of the triangular waveform, so that the dead time of the measurement is practically zero. Further details of the experimental setup, data acquisition and data preprocessing software can be found elsewhere[14]. All measurements are taken in the variable temperature insert of the commercially available Quantum Design Physical Property Measurement System (PPMS). PCAR spectroscopy is a performed in the temperature range 2.0 - 10.0 K. Measurements above the critical temperature of Nb ($T_{\mathrm{c}} = 9.2\,\mathrm{K}$) are used as normalization spectra and for corrections. PCS in high magnetic field ($\mu_0 H = 14\,\mathrm{T}$) is measured in order to study the density of states of the compositions. The temperature evolution of the zero-bias anomaly in the high-field PCS data is indicative of the insulating bulk behavior of the compositions at low temperature.

High-purity Bi(99.999 %), Sb(99.9999 %) and Te (99.9999 %) were evaporated from Knudsen effusion cells, and Cr(99.999 %) and V(99.995 %) were deposited by electron guns on heat-treated α-Al_2O_3(0001) substrates in a custom built molecular beam epitaxy system with a base pressure better than 5×10^{-10} torr. The compositions are determined by elements ratios obtained *in-situ* during growth using separate quartz crystal monitors. The TI thickness of each sample is 20 quintuple layerd (QL) and the surface is protected with 2 nm insulating Te capping layer[15]. This particular ternary topological insulator family $(Bi_{1-x}Sb_x)_2Te_3$ has been previously extensively studies by Zhang *et al.*[15]. The variation of Bi and Sb concentration drives the Fermi level from the bulk conduction band (Bi_2Te_3) into the bulk valence band (Sb_2Te_3). Respectively, the carriers are electrons and holes. At the optimized Bi:Sb ratio window, the Fermi level can be tuned into the bulk gap and approached to the Dirac point. The compensated sample exhibits semiconductor-like activation behavior upon cooling. Due to the high sheet resistance, the Sb_2Te_3 and $(Bi_{0.18}Sb_{0.82})_2Te_3$ samples are shadow masked with Al(40 nm)/Ag(30 nm). Bottom shunting layer[16] would not significantly reduce the sheet resistance in this case due to the significantly reduced bulk conductivity. Spin polarization in topological insulators is in plane and locked to the direction of the in-plane wave-vectors ($\vec{k}_{\mathrm{x}}$ and $\vec{k}_{\mathrm{y}}$). Statistically each electron of a Cooper pair has finite vertical projection of its spin. Furthermore, in the ballistic regime of PCAR (with small axial magnetic field) or alternatively in cases where there is a significant tunneling barrier and the injection is performed from a superconductor with finite spin-orbit coupling, Cooper pairs spins are aligned along the perpendicular wave-vector($\vec{k}_{\mathrm{z}}$). Cooper pairs are not allowed to be injected in topological insulators (due to momentum conservation within the elastic limit and at small bias) with spins along z, hence the Andreev reflection is suppressed and the contact shows high spin polarization. The measurement is a direct indication that the transport spin polarization is in plane. Since the PCAR probes contributions from both the surface and bulk states, an increase in spin polarization is to be expected, related to carrier depletion in the bulk, *i.e.* pronounced semi-metallic or semiconducting transport properties at low temperature. We observe exactly that, the spin polarization is higher for the compositions with larger bulk bandgap.

III. SPIN POLARISATION OF $(BI_{1-x}SB_x)_2TE_3$ FAMILY

PCAR spectra are measured in the temperature range from 2.0 K to 10.0 K. The conductances of most contacts are in the range 5.0 - 20.0 G_0. The high resistance of the point contacts is sought after because of two reasons: the transport current through the contact is kept in a quasi-ballistic regime, and the relative contribution of the TI sheet resistance is low. It has to be explicitly noted that reducing the point-contact resistance (increasing the effective contact area) leads to broadening of the spectral features and decreased value of the spin polarization. The analysis routine is based on Strijkers *et al.*[17] approach, although no significant proximity effect is observed in any of the contacts. The important extracted parameters from each fit are spin polarization P, barrier height Z, effective electronic temperature T_{e}, and the proximity gap Δ_1. The bulk superconducting gap of Nb, Δ_2, is kept constant. No significant proximity effect is present as the values of Δ_1 and Δ_2 are similar. Furthermore, additional five fitting parameters might be used : zero bias offset (x_{o}), conduction normalization offset(y_{o}), rescale of the conduction axis (y_{s}, due to pre-amplifier gain and sheet resistance), rescale of the voltage axis (x_{s}, due to sheet resistance), and quadratic background component

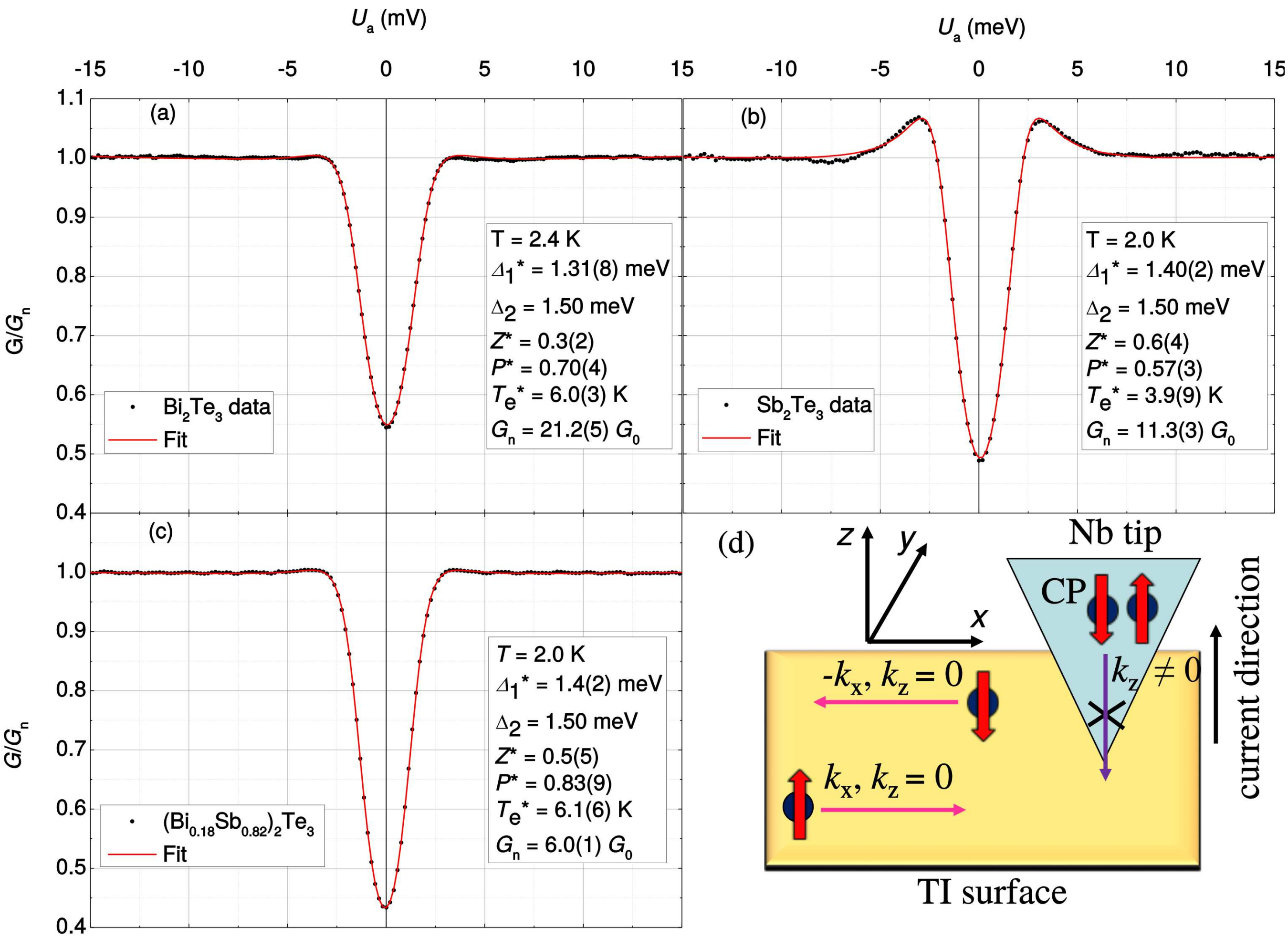

FIG. 1. PCAR spectra, fitting and extracted parameter for the three different compositions. (a) - Bi_2Te_3 with $P = 70(4)\,\%$, (b) - Sb_2Te_3 with $P = 57(3)\,\%$, and (c) - $(Bi_{0.18}S_{0.82})_2Te_3$ with $P = 83(9)\,\%$. The model extracted parameters are indicated with asterisks. Panel (d) represents the electron injection process in PCAR. The electron spins of the TI surface states are in-plane locked perpendicular to the momentum. Cooper pairs (CP) with out of plane spin components are not allowed to be injected elastically in the TI surface states due to momentum conservation.

(y_q, due to tunneling contributions). A multiparameter fit is susceptible to converging in local minima rather than the global solution and the uniqueness of the PCAR fit has been discussed before[18,19]. Our fitting procedure includes close-interval minimization and calculates the correlation and covariant matrices of the obtained fit in order to uncover interdependence between the parameters and the errors. An example is given on Fig. 4 (f). Three representative spectra along with the extracted fitting parameters for the three topological compositions (Bi_2Te_3, Sb_2Te_3, and $(Bi_{0.18}Sb_{0.82})_2Te_3$) are shown in Fig.(1). It has to be pointed out that all spectra exhibit small quadratic high bias background. The background is attributed to the DOS structure of the topological insulators and small tunneling current contribution. Previously extensive studies of the DOS bias dependence in topological insulators have been performed by scanning tunnelling microscopy[20,21]. Here, the energy scale is limited to the immediate (few meV) vicinity of the Fermi level. The PCAR spectra are normalized with spectra above the T_c of Nb. It has to be stated that the effective electronic temperature T_e is found to always be above the bath temperature of the setup T. The typical value for T_e is from 4.0 to 6.0 K, whereas the typical bath temperature T is from 2.0 to 2.4 K. Such electron heating and additional thermal broadening is often observed in PCAR of thin films[22], exception being only cases of cooling in low transparent superconducting tunnel junctions[23]. In this set of measurements, the elevated electronic temperature is mainly attributed to the formation of a narrow (tunneling-transparent) Schottky barrier at the tip-TI contact[24], which will be demonstrated later on Fig. 2 (c) and (d). The extracted spin polarization is 70(4), 57(3) and 83(9)%, respectively for the three compositions. In order to confirm that the observed spectral features are due to Andreev reflection, tempera-

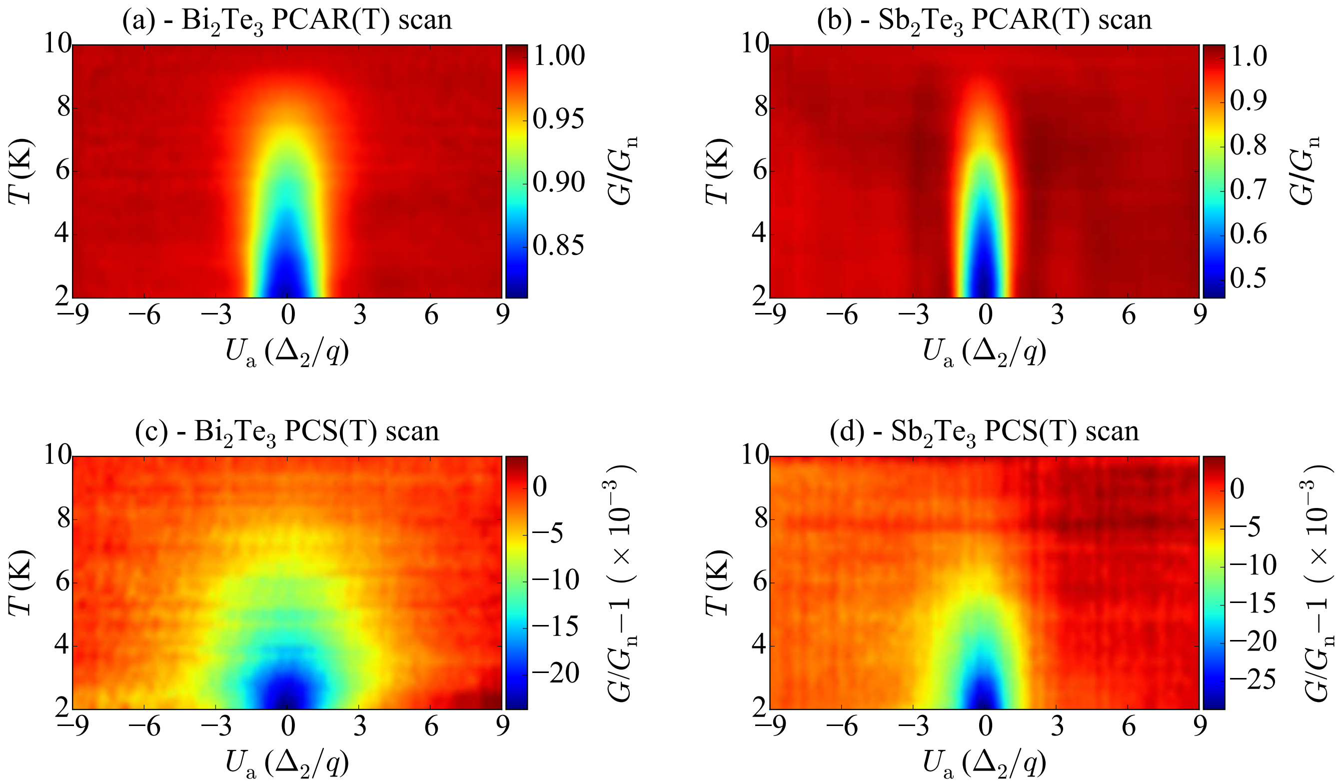

FIG. 2. Temperature scans of Bi_2Te_3 and Sb_2Te_3. (a) - PCAR spectra of Bi_2Te_3 between 2.0 to 10.0 K, (b) - PCAR spectra of Sb_2Te_3 between 2.0 to 10.0 K, (c) - PCS of Bi_2Te_3 in magnetic field of $\mu_0 H = 14\,$T, and (d) - PCS of Sb_2Te_3 in magnetic field of $\mu_0 H = 14\,$T, where $\Delta_2 = 1.5\,$meV is the bulk superconducting gap of Nb and q is the elementary charge.

ture scans of some of the contacts are recorded(Fig.(2)). The spectra are normalized with a background curve acquired at 10.0 K (above the critical temperature of Nb - $T_c = 9.2\,$K). PCAR temperature scans indicate the usual evolution of the spectra where the features become narrower and lower due to the reduction in the Nb superconducting gap combined with the temperature smearing; spectra are essentially flat above T_c. The last observation is a clear confirmation that the investigated samples demonstrate the expected high effective spin polarisation. Furthermore, the fact that Andreev signal is measured all the way to the critical temperature of Nb (see Fig. (3) (a) and (b)) is a clear demonstration that the transport is elastic and there is no appreciable Joule heating in the contact area. Once the superconducting tip is quenched (either in high magnetic field or at high temperature) and provided that the density of states around the Fermi level ($\approx \pm 15\,$meV) is featureless, the point-contact spectroscopy (PCS) must exhibit a flat line. Interestingly, spectra exhibit really structure in magnetic field above the upper critical field of Nb. As the magnetic field is scanned from 0 to 14 T, the spectral features change from the well-established Andreev reflection structure to a Lorentzian-like shape. The latter is an indication of carrier depletion and existence of small band gap in the bulk density of states of the topological insulators. The conductance features of the PCS are an order of magnitude smaller than the features of the PCAR. Hence, contribution from the carrier depletion towards the overall PCAR signal is considered insignificant for the analysis of the spin polarization. The high-field PCS demonstrates essentially the differential conductance of the tunneling barrier between the Nb tip and the TI sample. The zero bias anomaly (ZBA) of the PCS temperature scans (Fig. (2) c and d) decays much faster than the ZBA of the PCAR temperature scans (Fig. (2) a and b) as temperature is increased. The temperature evolution of the ZBA in PCS decays exponentially following Arrhenius law. On the other hand, the ZBA of PCAR should follow the Bardeen-Cooper-Schrieffer (BCS)[25,26] evolution of the superconducting gap, provided that the density of states (DOS) of the studied material are flat within the DC bias range. The critical exponent of the superconducting transition in the weak-coupling regime following the BCS-theory is $\gamma = 0.5$[25,26]. The extracted critical exponents for the transitions of the Bi_2Te_3/Nb and Sb_2Te_3/Nb contacts are significantly higher : 0.91(2) and 0.71(2), respectively. The deviation from the BCS bahaviour is due to formation of a narrow Schottky barrier and that the spin polarisation is efficient Cooper pair breaker[27]. A consequence of this is that the effective electronic temperature is significantly above the bath tem-

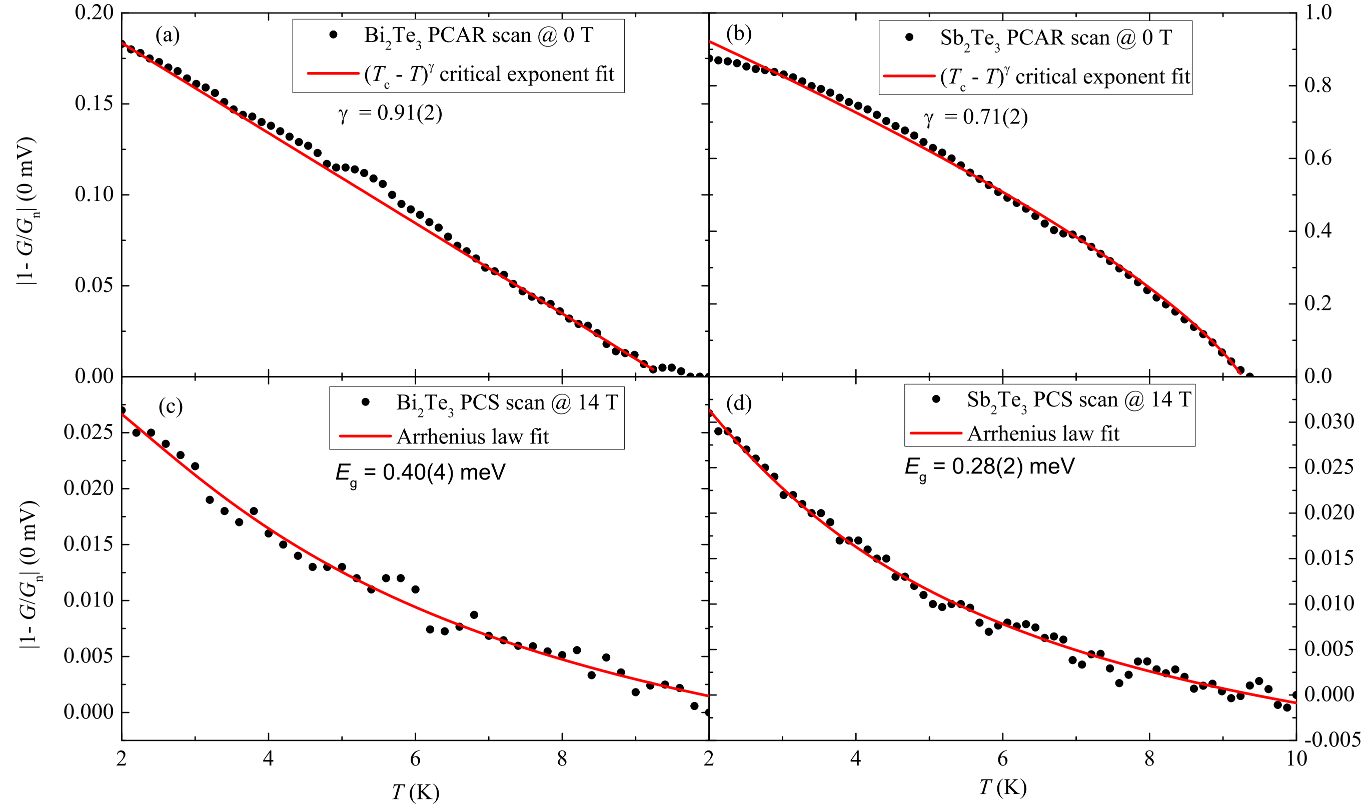

FIG. 3. Temperature evolution of the ZBA of PCAR (top panels) and PCS (bottom panels) along with extracted critical exponents (γ) of the superconducting transition and the bulk band gap (E_g). (a) - ZBA of the PCAR temperature scan in zero magnetic field of Bi_2Te_3 with $\gamma = 0.91(2)$, (b) - ZBA of the PCAR temperature scan of Sb_2Te_3 in zero magnetic field with $\gamma = 0.71(2)$, (c) - ZBA of the PCS temperature scan of Bi_2Te_3 in $\mu_0 H = 14$ T with $E_g = 0.40(4)$ meV, and (d) - ZBA of the PCS temperature scan of Sb_2Te_3 in $\mu_0 H = 14$ T with $E_g = 0.28(2)$ meV. The presented ZBA plots are extracted from the ZBA temperature dependence in Fig. (2).

perature (injection occurs above the Fermi level). Furthermore, as these materials exhibit very small gap at low temperatures, the observed energy gap evolves significantly from 2 to 10 K, and the T_e does not follow linearly the increase in T.

The temperature evolution of ZBA of PCS in $\mu_0 H = 14$ T is presented in Fig. (3). The ZBA temperature evolutions in high field (bottom panels on Fig. (3)) is in contrast with the ZBA temperature scans in zero field (top panels on Fig. (3)). Our very high field PCS ($\mu_0 H = 14$ T) demonstrates small bulk bandgaps for both compositions. The Arrhenius fitting of the data gives $E_g = 0.28(2)$ meV and 0.40(4) meV, respectively for Sb_2Te_3 and Bi_2Te_3. The larger gap of Bi_2Te_3 correlates with the measured higher spin polarization. In fact, resistance upturn at very low temperatures has already been reported for these compositions[15]. It is important to note that the observed gap should not be directly linked to the gap in the TI electronic structure. The Nb tip might introduce disorder (vacancies, dislocations etc.) in the crystal structure, and, hence, alter the density of states. The work of Jiang *et al.*[28] has demonstrated that the bulk gap in Sb_2Te_3 decreases with increasing the thickness of the TI sample. Furthermore, these compositions exhibit close to degenerate semiconducting behavior with the Fermi level positioned in the vicinity of the conduction or the valence band edges, respectively. Therefore, the extracted gaps demonstrate the energy spacing between the Fermi level and the corresponding band edge rather than the full band gap. The determined bulk band gap in these samples is 100 meV-200 meV[15]. The larger extracted gap of Bi_2Te_3 correlates with the higher value of critical exponent extracted from the PCAR temperature dependence (see Fig. (3)c). This observation of high-field PCS is an explicit demonstration of carrier depletion in these topological insulators.

It is important to comment on the full field scan of a Bi_2Te_3/Nb point contact(Fig. (5)). The low field scan indicates that the Andreev-reflection features disappear in small field $\mu_0 H \approx 0.5$ T. The contact quench field is on par with the bulk upper critical field H_{c3} of Nb[29] and within the error expected for the lack of proper polycrystalline average within the point contact ($\pm$ 36%)[30]. As was the case with the temperature evolution, the field evolution of the superconducting gap does not follow the expected BCS evolution. The reasons are likely related to the highly spin polarized current through the contact[27]. Furthermore, the full field scan indicates that the ZBA is relatively field insensitive from the quench field ($\mu_0 H = 0.5\,\mathrm{T}$) up to the maximum available field $\mu_0 H = 14\,\mathrm{T}$. The effective field scale over which the conductance dip diminishes is about $\mu_0 H = 10\,\mathrm{T}$, which corresponds to Zeeman splitting of approximately 0.92 meV or narrowing of the gap, very close to the one observed by thermal activation in Fig. (3). This could be interpreted as either the inelastic tunneling between two states (one in the valence part and one in the conduction part of the Dirac cone) at constant momentum, or potentially the spin-orbit splitting of a bulk conduction state at the Fermi level.

IV. SPIN POLARISATION OF MAGNETICALLY-DOPED TOPOLOGICAL INSULATORS

We further investigate the effect of magnetic ions doping on the spin polarization of Bi_2Te_3, and Sb_2Te_3. Magnetic topological insulators have been realized by Cr- and V-doping[31,32]. Recently, high Curie temperature and robust Quantum Anomalous Hall Effect (QAHE) were observed in optimally V-doped TIs[33]. Both Cr and V are substitutional on the Bi(Sb) sublattice. While V acts as electron donor[33] in Sb_2Te_3, the contribution of carriers by Cr doping is smaller but hole type[31,34] in the same parent compound. The carrier concentration in the Cr-Bi_2Te_3 should be reduced and the spin polarization increased. Contrarily, Cr-doping was shown to decrease the spin polarization of the Bi_2Te_3 composition which is attributed to spin-flip scattering effect from paramagnetic impurities[35]. On the other hand, Cr-doping of Sb_2Te_3 is expected to affect very little or to slightly increase the bulk hole carrier concentration, which should lead to lower spin polarization compared with the pure Sb_2Te_3 sample. Decreased spin polarization is indeed measured in this composition. The extracted spin polarization of $Bi_{1.97}Cr_{0.03}Te_3$ and $Sb_{1.975}Cr_{0.025}Te_3$ is 52(1) % and 52(1) %. Vanadium doping has been shown to induce harder magnetism and higher Curie temperature than chromium[33]. V-doped Bi_2Te_3 demonstrated a lower spin polarization value of $P = 58(5)\,\%$ than the pristine composition. Three of the measured compositions do not demonstrate magnetic ordering : $Bi_{1.97}Cr_{0.03}Te_3$, $Sb_{1.975}Cr_{0.025}Te_3$, and $Bi_{1.975}V_{0.025}Te_3$. The decreased values of the spin polarization is due to spin-flip scattering by paramagnetic impurities[36]. Non-magnetic impurities and disorder do not cause backscattering of electrons from the TI surface states[37], however, doping with magnetic ions must result in spin-flip scattering[35]. $Sb_{1.97}V_{0.03}Te_3$ is the only composition which demonstrates magnetic behaviour in the measurement temperature range ($T > 2.0\,\mathrm{K}$). The extra free electrons, provided by the vanadium, reduce the natural p-type character of the original composition and this should result in a lower bulk conduction and higher contribution of the surface carriers towards the measured spin polarization. However, it exhibits the lowest value of spin polarization ($P = 50\,\%$). The decreased spin polarization in the magnetically-ordered sample is attributed to the fact that the magnetic easy axis is perpendicular to plane (as evidenced by AHE) whereas the spins of the electrons in the TIs surface state are usually locked in the plane. This must increase the electron-electron spin scattering and via the Kramers-Kronig relations reduce the density of surface states and their bulk penetration thus impacting the overall effective spin polarization as perceived by PCAR. No features similar to the PCS in Fig. (1 (c) and (d)) have been observed in the magnetically doped samples[38,39]. The ferromagnetic ordering of all compositions is probed by Anomalous Hall Effect (AHE) in van der Pauw configuration. Only $Sb_{1.97}V_{0.03}Te_3$ demonstrated AHE signal at temperature of 2.0 K or higher. The AHE amplitude of the latter composition is evaluated as a function of temperature and the Curie temperature of $T_C = 11.6(6)\,\mathrm{K}$ determined (see Fig. (4)e).

V. CONCLUSIONS

The high in-plane spin polarization in the topological insulator family $(Bi_{1-x}Sb_x)_2Te_3$ is verified by a direct electrical measurement. The measured spin polarization is in the range of 60 to 85 % and represents a low limit for the intrinsic spin polarization in these topological insulators. Various artefacts stay in the way of a more accurate determination: tip induced damage, directionality of the current, not-fully ballistic transport and interfacial spin-flip events at the topological insulator/superconductor interface. It has to be emphasized that the value is obtained at 2 K, and no temperature dependence of the spin polarization is studied due to the limitations of PCAR imposed by the low-critical temperature of Nb. Carrier depletion by direct point contact spectroscopy was demonstrated for first time. The extracted bulk bandgaps of Bi_2Te_3 and Sb_2Te_3 correlate with the expectation that higher bulk carrier depletion results in higher effective spin polarisation. Furthermore, we investigated the influence of magnetic ions on the spin polarization of four topological insulator compositions : $Bi_{1.97}Cr_{0.03}Te_3$, $Sb_{1.975}Cr_{0.025}Te_3$, $Bi_{1.975}V_{0.025}Te_3$, and $Sb_{1.97}V_{0.03}Te_3$. Low doping concentration, insufficient to induce ferromagnetic behaviour, was shown to reduce the value of the spin polarization. The latter demonstrates that paramagnetic ions act as spin-flip scattering centers and decrease the TI surface states spin polarization[35]. The only ferromagnetic composition among the four, $Sb_{1.97}V_{0.03}Te_3$, had the lowest spin polarization which is attributed to the competition between in-plane spin locking and perpendicular magnetic anisotropy. Extensions of the current investigation should permit the measurement of the spin polarization of optimally V-doped Sb_2Te_3, the tracking of the spin polarization as a func-

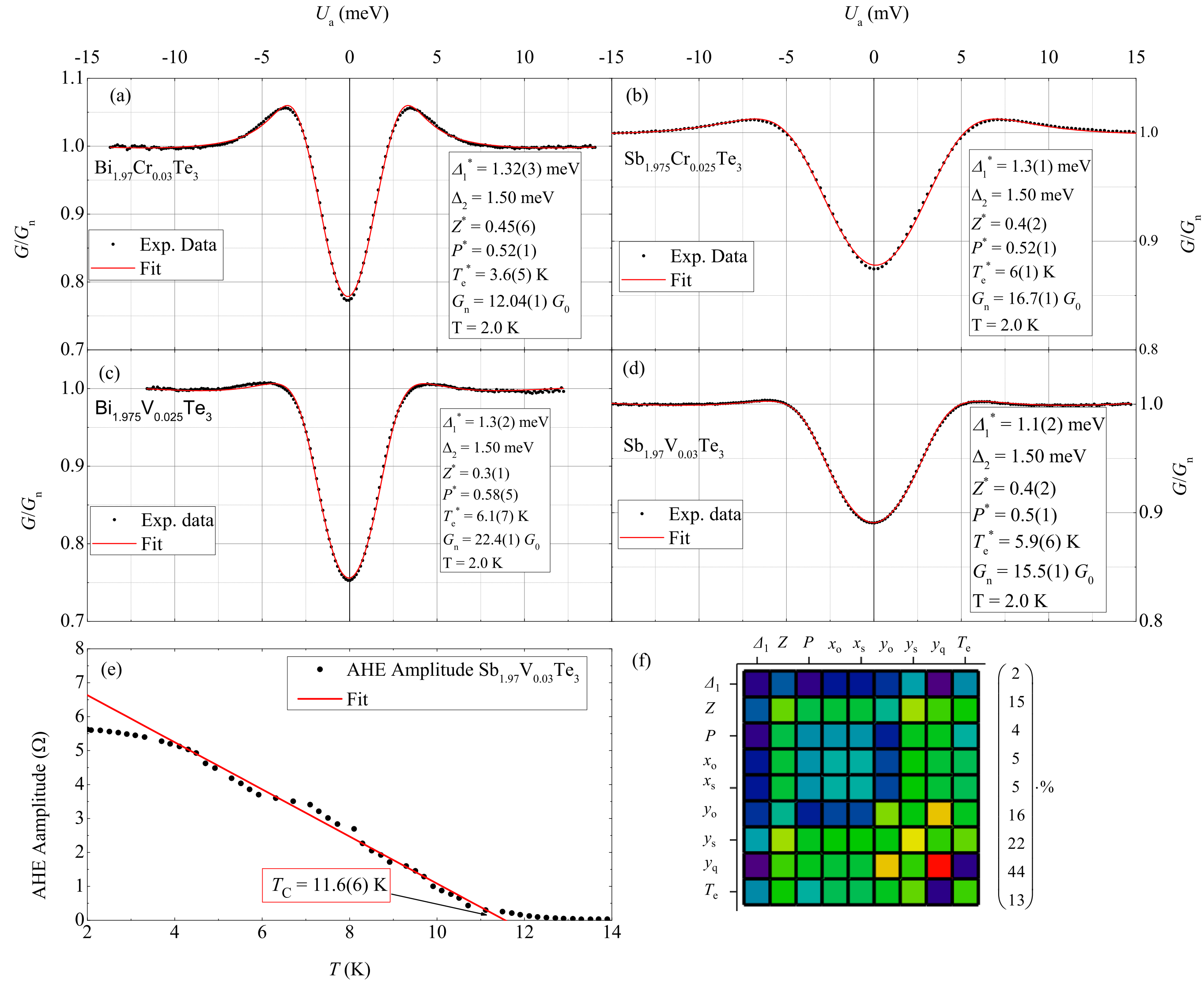

FIG. 4. Fitted PCAR data along with the extracted parameters of four magnetically doped TI compositions. Panel (a) shows $Bi_{1.97}Cr_{0.03}Te_3$, Panel (b) - $Sb_{1.975}Cr_{0.025}Te_3$, Panel (c) - $Bi_{1.975}V_{0.025}Te_3$, Panel (d) - $Sb_{1.97}V_{0.03}Te_3$, Panel (e) - AHE temperature scan of $Sb_{1.97}V_{0.03}Te_3$ with the extracted Curie temperature of $T_C = 11.6(6)$ K. Panel (f) - example of a covariant matrix on the fit on Panel (a) and the vector of the parameters errors.

tion of the applied gate bias, and the evaluation of the spin polarization in the QAHE regime.

ACKNOWLEDGMENTS

K. B. and P. S. would like to acknowledge financial support from Science Foundation Ireland within SSPP (11/SIRG/ I2130), NISE (10/IN1/I3002) and AMBER programme. K. B. would like to further thank the 2016 Joint MMM-Intermag Steering Committee for the provided Student Travel Grant which facilitate the presentation of this work. C.Z.C and J.S.M. acknowledge support from grants NSF (DMR-1207469), NSF (DMR-0819762) (MIT MRSEC), ONR (N00014-13-1-0301), and the STC Center for Integrated Quantum Materials under NSF grant DMR-1231319.

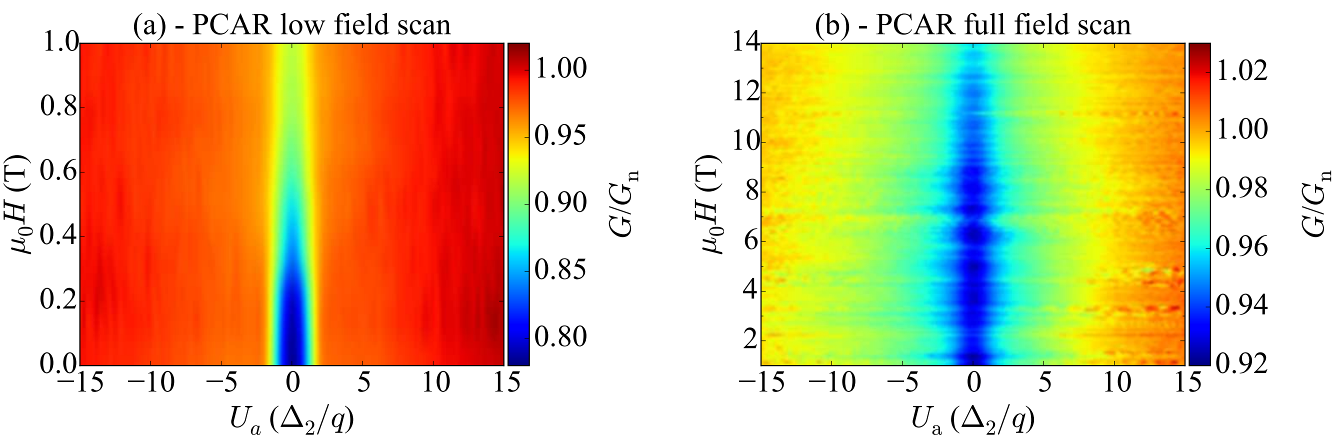

FIG. 5. Magnetic field scan of a Bi_2Te_3/Nb point contact at 2.0 K. Left panel represents the low-field scan up to $\mu_0 H = 1.0\,\mathrm{T}$ and the right panel represents the high-field scan from 1 T up to $\mu_0 H = 14.0\,\mathrm{T}$. Where $\Delta_2 = 1.5\,\mathrm{meV}$ is the bulk superconducting gap of Nb and and q is the elementary charge.

* borisovk@tcd.ie

[1] M. Z. Hasan and C. L. Kane, Rev. Mod. Phys. **82**, 3045 (2010).
[2] H. van Leuken and R. A. de Groot, Phys. Rev. Lett. **74**, 1171 (1995).
[3] H. Kurt, K. Rode, P. Stamenov, M. Venkatesan, Y.-C. Lau, E. Fonda, and J. M. D. Coey, Phys. Rev. Lett. **112**, 027201 (2014).
[4] Y. Fan, P. Upadhyaya, X. Kou, M. Lang, S. Takei, Z. Wang, J. Tang, L. He, L.-T. Chang, M. Montazeri, G. Yu, W. Jiang, T. Nie, R. N. Schwartz, Y. Tserkovnyak, and K. L. Wang, Nat Mater **13**, 699 (2014).
[5] Y. Fan, X. Kou, P. Upadhyaya, Q. Shao, L. Pan, M. Lang, X. Che, J. Tang, M. Montazeri, K. Murata, L.-T. Chang, M. Akyol, G. Yu, T. Nie, K. Wong, J. Liu, Y. Wang, Y. Tserkovnyak, and K. Wang, Nature Nanotechnology **11**, 352 (2016).
[6] D. Hsieh, Y. Xia, D. Qian, L. Wray, F. Meier, J. H. Dil, J. Osterwalder, L. Patthey, A. V. Fedorov, H. Lin, A. Bansil, D. Grauer, Y. S. Hor, R. J. Cava, and M. Z. Hasan, Phys. Rev. Lett. **103**, 146401 (2009).
[7] Y. Ando, T. Hamasaki, T. Kurokawa, K. Ichiba, F. Yang, M. Novak, S. Sasaki, K. Segawa, Y. Ando, and M. Shiraishi, Nano Letters **14**, 6226 (2014), http://dx.doi.org/10.1021/nl502546c.
[8] J. Tang, L.-T. Chang, X. Kou, K. Murata, E. S. Choi, M. Lang, Y. Fan, Y. Jiang, M. Montazeri, W. Jiang, Y. Wang, L. He, and K. L. Wang, Nano Letters **14**, 5423 (2014), http://dx.doi.org/10.1021/nl5026198.
[9] C. Li, O. Van't Erve, J. Robinson, Y. Liu, L. Li, and B. Jonker, Nature Nanotechnology **9**, 218 (2014).
[10] A. Dankert, J. Geurs, M. V. Kamalakar, S. Charpentier, and S. P. Dash, Nano Letters **15**, 7976 (2015), pMID: 26560203, http://dx.doi.org/10.1021/acs.nanolett.5b03080.
[11] P. M. Tedrow and R. Meservey, Phys. Rev. Lett. **26**, 192 (1971).
[12] R. Soulen Jr, M. Osofsky, B. Nadgorny, T. Ambrose, P. Broussard, S. Cheng, J. Byers, C. Tanaka, J. Nowack, J. Moodera, *et al.*, Journal of applied physics **85**, 4589 (1999).
[13] I. Mazin, Physical Review Letters **83**, 1427 (1999).
[14] P. Stamenov, Journal of Applied Physics **113**, 17C718 (2013), http://dx.doi.org/10.1063/1.4796049.
[15] J. Zhang, C.-Z. Chang, Z. Zhang, J. Wen, X. Feng, K. Li, M. Liu, K. He, L. Wang, X. Chen, Q.-K. Xue, X. Ma, and Y. Wang, Nature Communications **2** (2011), 10.1038/ncomms1588.
[16] L. Bocklage, J. M. Scholtyssek, U. Merkt, and G. Meier, Journal of Applied Physics **101**, 09J512 (2007), http://dx.doi.org/10.1063/1.2710238.
[17] G. J. Strijkers, Y. Ji, F. Y. Yang, C. L. Chien, and J. M. Byers, Phys. Rev. B **63**, 104510 (2001).
[18] Y. Bugoslavsky, Y. Miyoshi, S. K. Clowes, W. R. Branford, M. Lake, I. Brown, A. D. Caplin, and L. F. Cohen, Phys. Rev. B **71**, 104523 (2005).
[19] V. Baltz, A. D. Naylor, K. M. Seemann, W. Elder, S. Sheen, K. Westerholt, H. Zabel, G. Burnell, C. H. Marrows, and B. J. Hickey, Journal of Physics: Condensed Matter **21**, 095701 (2009).
[20] A. Soumyanarayanan and J. E. Hoffman, Journal of Electron Spectroscopy and Related Phenomena **201**, 66 (2015).
[21] Y. Okada, C. Dhital, W. Zhou, E. D. Huemiller, H. Lin, S. Basak, A. Bansil, Y.-B. Huang, H. Ding, Z. Wang, S. D. Wilson, and V. Madhavan, Phys. Rev. Lett. **106**, 206805 (2011).
[22] S. Rajauria, P. Gandit, T. Fournier, F. W. J. Hekking, B. Pannetier, and H. Courtois, Phys. Rev. Lett. **100**, 207002 (2008).
[23] S. Rajauria, P. S. Luo, T. Fournier, F. W. J. Hekking, H. Courtois, and B. Pannetier, Phys. Rev. Lett. **99**, 047004 (2007).
[24] A. W. Kleinsasser, T. N. Jackson, D. McInturff, F. Rammo, G. D. Pettit, and J. M. Woodall, Applied Physics Letters **57** (1990).
[25] J. Bardeen, L. N. Cooper, and J. R. Schrieffer, Phys. Rev. **108**, 1175 (1957).
[26] P. Townsend and J. Sutton, Phys. Rev. **128**, 591 (1962).
[27] D. Kumar, P. C. Joshi, Z. Hossain, and R. C. Budhani, Applied Physics Letters **102**, 112409 (2013), http://dx.doi.org/10.1063/1.4798286.
[28] Y. Jiang, Y. Wang, M. Chen, Z. Li, C. Song, K. He, L. Wang, X. Chen, X. Ma, and Q.-K. Xue, Phys. Rev. Lett. **108**, 016401 (2012).
[29] V. Karasik and I. Shebalin, SOV PHYS JETP **30**, 1068 (1970).
[30] H. R. Kerchner, D. K. Christen, and S. T. Sekula, Phys. Rev. B **24**, 1200 (1981).
[31] J. S. Dyck, P. Hájek, P. Lošt'ák, and C. Uher, Phys. Rev. B **65**, 115212 (2002).
[32] P. P. J. Haazen, J.-B. Lalo, T. J. Nummy, H. J. M. Swagten, P. Jarillo-Herrero, D. Heiman, and J. S. Moodera, Applied Physics Letters **100**, 082404 (2012), http://dx.doi.org/10.1063/1.3688043.
[33] C.-Z. Chang, W. Zhao, D. Y. Kim, H. Zhang, B. A. Assaf, D. Heiman, S.-C. Zhang, C. Liu, M. H. W. Chan, and J. S. Moodera, Nat Mater **14**, 473 (2015).
[34] C.-Z. Chang, J. Zhang, M. Liu, Z. Zhang, X. Feng, K. Li, L.-L. Wang, X. Chen, X. Dai, Z. Fang, X.-L. Qi, S.-C. Zhang, Y. Wang, K. He, X.-C. Ma, and Q.-K. Xue, Advanced Materials **25**, 1065 (2013).
[35] L. A. Wray, S.-Y. Xu, Y. Xia, D. Hsieh, A. V. Fedorov, Y. S. Hor, R. J. Cava, A. Bansil, H. Lin, and M. Z. Hasan, Nat Phys **7**, 32 (2011).
[36] F. Yang, Y. R. Song, H. Li, K. F. Zhang, X. Yao, C. Liu, D. Qian, C. L. Gao, and J.-F. Jia, Phys. Rev. Lett. **111**, 176802 (2013).
[37] P. Roushan, J. Seo, C. Parker, Y. Hor, D. Hsieh, D. Qian, A. Richardella, M. Hasan, R. Cava, and A. Yazdani, Nature **460**, 1106 (2009).
[38] Q. Liu, C.-X. Liu, C. Xu, X.-L. Qi, and S.-C. Zhang, Phys. Rev. Lett. **102**, 156603 (2009).
[39] J. Sanchez-Barriga, A. Varykhalov, G. Springholz, H. Steiner, R. Kirchschlager, G. Bauer, O. Caha, E. Schierle, E. Weschke, A. A. Unal, S. Valencia, M. Dunst, J. Braun, H. Ebert, J. Minar, E. Golias, L. V. Yashina, A. Ney, V. Holy, and O. Rader, Nat Commun **7** (2016), article.